Unique Nonlinear Behavior of Nano-Filled Elastomers: From the Onset of Strain Softening to Large Amplitude Shear Deformations

ARTICLE *in* MACROMOLECULES · MARCH 2012

Impact Factor: 5.8 · DOI: 10.1021/ma202278e

7 AUTHORS, INCLUDING:

Samy Merabia
French National Centre for Scientific Research
47 PUBLICATIONS **515** CITATIONS

Macromolecules

Article

pubs.acs.org/Macromolecules

Unique Nonlinear Behavior of Nano-Filled Elastomers: From the Onset of Strain Softening to Large Amplitude Shear Deformations

Aurélie Papon,[†] Samy Merabia,*[,‡] Laurent Guy,[§] François Lequeux,[†] Hélène Montes,[†] Paul Sotta,[⊥] and Didier R. Long*[,⊥]

[†]Physico-Chimie des Polymères et Milieux Dispersés, ESPCI ParisTech, 10 rue Vauquelin, F-75231 Paris Cedex 5, France

[‡]Laboratoire de Physique de la Matière Condensée et Nanostructures, Université Lyon I/CNRS, 43 Boulevard du 11 Novembre 1918, 69622 Villeurbanne Cedex, France

[§]Rhodia Opérations, 15 rue Pierre Pays, BP 52, F-69660 Collonges-au-Mont-d'Or, France

[⊥]Laboratoire Polymères et Matériaux Avancés, CNRS/Rhodia, 85 avenue des Frères Perret, F-69192 Saint-Fons, France

ABSTRACT: Adding fillers in elastomers is known to increase the elastic modulus and the wear resistance of elastomers, but also to increase nonlinear dissipation, a phenomenon known as the Payne effect. Indeed, when submitted to deformations of the order of a few per cents or more, the elastic modulus can decrease down to values much smaller than the initial one. On the other hand, when submitted to large amplitude oscillatory shear at a frequency ω, frequency analysis shows that the contribution of higher harmonics 3ω, 5ω, ..., to the response is quite small. This might appear somehow as a paradox since the nonlinear behavior of filled elastomers can be strongly marked. We discuss here in detail a possible physical origin of these various features. We do it by comparing experimental results performed on model elastomers to the prediction of a model proposed recently, based on the presence of glassy bridges linking neighboring particles. We show that the kinetics of rupture and rebirth of these glassy bridges can explain these effects.

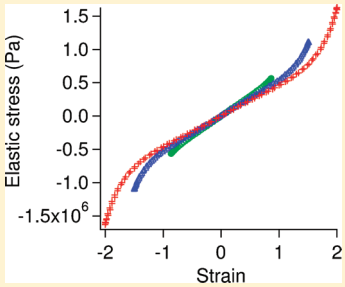

I. INTRODUCTION

Filled elastomers are systems of very great practical importance, due to their unique properties. Nonreinforced polymer matrices generally do not exhibit mechanical properties suitable for some practical purposes, being too soft and fragile.[1] On the contrary, elastomers filled with carbon black or silica particles have a shear modulus much (up to a few 100 times) higher than that of the pure elastomer, exhibit a high dissipative efficiency, and are extremely resistant to both fracture and abrasion, which makes them highly useful for damping materials, shock absorbers, or tires.[1−13]

When submitted to periodic deformations at a frequency ω of typical order of magnitude 1 Hz, and of amplitudes γ_0 of the order of a few per cents or more, the apparent elastic modulus $G'(\omega,\gamma_0)$ decreases down to values much smaller than the value in the linear regime; this is the so-called Payne effect. In some systems studied by Payne, the modulus dropped from a few 10^7 Pa down to a few 10^6 Pa.[8] Conversely, in an unfilled matrix, a roughly constant modulus is observed until 100% of strain.[6,8,9,12,14−18] After the system has been put at rest and during subsequent deformations, the elastic modulus in the linear regime is smaller than that of the initial system, but recovers progressively—at least partially—the initial value.[5,19] It is an issue of major importance to understand this unique behavior in order to be able to control and tune the properties of these systems. These effects cannot be simply explained by the trivial geometric role of the solid particles, but must involve the modification of the polymer dynamics near the solid interface, which leads for example to the Payne effect.[10,11,13]

We proposed recently that these effects are the consequence of the presence of a glassy layer around the fillers, which can build glassy bridges between neighboring fillers.[20−24] Indeed, it had long been proposed that the polymer matrix in the vicinity of the filler is glassy.[11,25−30] This picture is also consistent with experimental studies that demonstrated that the glass transition temperature T_g in thin polymer films in contact with a solid substrate differs from the one in the bulk, in a way that depends on the polymer−substrate interaction.[31−40] The link between glass transition in thin films and physical properties of nanocomposites has been emphasized by many other authors.[41−49] The model we propose, the glassy bridge reinforcement model (GBRM), has provided a unified picture to account for (1) reinforcement amplitudes, (2) the Payne effect, (3) recovery effects, and (4) specific features of the plastic properties of filled elastomers.[50−52]

As regards mechanical properties, it is often thought that a nonlinear behavior under periodic solicitations at frequency ω would result in contributions to the response at higher frequency harmonics 3ω, 5ω, ... In particular, this is the case when the stress σ is a nonlinear, nonretarded function of the deformation x with a constitutive relation of the type: $\sigma(x) = k^{(1)}x + k^{(3)}x^3 + k^{(5)}x^5 + ...$ On the other hand, regarding filled elastomers, it has

Received: October 12, 2011
Revised: February 23, 2012
Published: March 9, 2012

been reported that, whereas the storage modulus can be much smaller than the small amplitude linear modulus, the response is still quasi-harmonic: if the applied strain is a sine wave, the measured stress is also a quasi-sinusoidal wave with small higher harmonic components.[53−56] This might thus appear somehow as a paradox. In addition, some of us have recently shown[57] that a significant deviation from the quasi-harmonic behavior can be measured in model samples. It is therefore important to clarify this feature, and also to check whether the model we have proposed for explaining the reinforcement and the Payne effect can also explain this behavior.

For describing the response of filled elastomers, we have argued that a key feature is the dynamical state of the glassy bridges.[50,51] It is characterized by a relaxation time, or lifetime, which is assumed to depend on the distance between the fillers, the polymer/filler interactions, the local stress value and history. The presence of a local stress in between the fillers leads to a reduction of the local glass transition temperature and an acceleration of the local dynamics. When the stress is released after local plastic deformation, physical aging takes place. The lifetime of the glassy bridge increases again. These features result in a complex history dependence of the dynamical state of the glassy bridges. In a permanent regime of sinusoidal deformation, the storage and dissipative moduli depend on the distribution of the lifetimes of glassy bridges in the system. The purpose of this paper is to study in more detail some specific aspects of the nonlinear behavior regarding both the storage and the dissipative moduli, and also how the higher harmonic contributions depend on strain amplitude and temperature. To this aim, we compare experimental results to the predictions of the glassy bridge reinforcement model and show that they match qualitatively. It is important to stress that no modification has been implemented in the model as compared to our previous works[50,51] in which the reinforcement mechanisms, the Payne and Mullins effects and the plastic behavior as deduced from the model were studied in detail. Thus, everything that was put forward in these previous papers remains valid for the simulations considered here.

The paper is organized as follows. In section II, we define in a precise way the studied quantities. Section III is the experimental part of the paper. The experimental model systems are described and their nonlinear response to large amplitude oscillatory strain (LAOS) is discussed. Section IV is the theoretical part of the paper. The physical ingredients of the GBRM and its numerical resolution are recalled. In section V, we present the results of the simulations and we discuss and compare them to the experimental data in section VI.

II. DEFINITION OF THE NONLINEAR PROBLEM

Here we aim at quantifying in detail the nonlinear behavior of filled elastomers submitted to large amplitude sinusoidal deformations. Both the in-phase and out-of phase response need to be defined in the nonlinear regime. The method is briefly described starting from the linear case, and then generalized to the nonlinear case. Following Cho et al.,[58] as well as some other authors[54,55,59−64] (see also ref 65 for review), the stress is decomposed into an elastic and a viscous part. In the linear regime, the stress ensuing a sinusoidal strain $\gamma(t)$ can classically be written as

$$\sigma(t) = G'\gamma(t) + G''\dot{\gamma}(t)/\omega \tag{1}$$

It is the sum of two terms: one in-phase with the strain corresponding to the elastic response $\sigma' = G'\gamma$ and one in quadrature with the strain corresponding to the viscous response $\sigma'' = G''\dot{\gamma}/\omega$. Thus, for an applied strain $\gamma = \gamma_0 \sin(\omega t)$, the elastic stress σ' is a sine wave—odd part—and the viscous part σ'' a cosine—even part. Then, when σ' is plotted as a function of γ—respectively σ'' as a function of $\dot{\gamma}/\omega$—a straight line with a slope G'—respectively G'' is obtained.

If a large amplitude sinusoidal strain is applied, the measured stress can be non sinusoidal, but it is still periodic. It can be decomposed in a unique way into odd−σ' and even−σ'' parts:

$$\sigma(t) = \sigma'(t) + \sigma''(t) \tag{2}$$

with

$$\sigma'(t) = (\sigma(t) - \sigma(-t))/2 \tag{3}$$

$$\sigma''(t) = (\sigma(t) + \sigma(-t))/2 \tag{4}$$

An analysis may be performed in the frequency domain. For an applied deformation $\gamma(t) = \gamma_0 \sin(\omega t)$, the in-phase and out-of phase stress responses $\sigma'(t)$ and $\sigma''(t)$ are given respectively by

$$\sigma'(t) = \sum_{n=1}^{\infty} a_n(\omega, \gamma_0) \sin(n\omega t) \tag{5}$$

$$\sigma''(t) = \sum_{n=1}^{\infty} b_n(\omega, \gamma_0) \cos(n\omega t) \tag{6}$$

Because σ' and σ'' are odd functions of γ and $\dot{\gamma}$ respectively, a_n and b_n are nonzero only for odd values of n. The most straightforward way to expand σ' and σ'' as functions of the instantaneous strain and instantaneous strain rate, respectively, has been described recently by Ewoldt et al[61] and is

$$\sigma'(x) = \gamma_0 \sum_{n:\text{odd}}^{\infty} e_n(\omega, \gamma_0) T_n(x) \tag{7}$$

$$\sigma''(y) = \gamma_0\omega \sum_{n:\text{odd}}^{\infty} v_n(\omega, \gamma_0) T_n(y) \tag{8}$$

where $T_n(x)$ is the nth order Chebyshev polynomial of the first kind, with $x = \gamma/\gamma_0$ and $y = \dot{\gamma}/\dot{\gamma}_0$. These polynomials are defined by

$$T_n(\cos\theta) = \cos(n\theta) \tag{9}$$

and satisfy the relation $T_n(\sin\theta) = \sin(n\theta)(-1)^{(n-1)/2}$ (n: odd). Some more details are given in Appendix. With these notations, one has the following relations:

$$\begin{aligned} \gamma_0 e_n(\omega, \gamma_0) &= a_n(\omega, \gamma_0)(-1)^{(n-1)/2} \quad n\text{: odd} \\ \gamma_0\omega v_n(\omega, \gamma_0) &= b_n(\omega, \gamma_0) \quad n\text{: odd} \end{aligned} \tag{10}$$

The dissipated energy per period is

$$W = \int_0^T \sigma''(t)\dot{\gamma}\, dt = \gamma_0 b_1(\omega, \gamma_0)\pi \tag{11}$$

dx.doi.org/10.1021/ma202278e | Macromolecules 2012, 45, 2891−2904

where $T = 2\pi/\omega$ is the period. W depends only on $b_1(\gamma_0,\omega)$. In,[50,51] the nonlinear dependence of the first harmonics (which dominates the response) was computed by the GBRM:

$$G'(\omega,\gamma_0) = \frac{a_1(\omega,\gamma_0)}{\gamma_0} = e_1(\omega,\gamma_0)$$
$$G''(\omega,\gamma_0) = \frac{b_1(\gamma_0,\omega)}{\gamma_0} = \omega v_1(\omega,\gamma_0) \quad (12)$$

and was then discussed and compared to the results published by Payne. However, in experimental data obtained in,[57] other non linear terms clearly reveal a specific behavior of filled rubbers. Therefore, in this paper the whole nonlinear dependence of σ' and σ'' as a function of the deformation amplitude is considered and compared to experimental data. It is given by the expansion

$$\sigma'(t) = \gamma_0\left(e_1(\omega,\gamma_0)\frac{\gamma(t)}{\gamma_0} + e_3(\omega,\gamma_0)\left(4\left(\frac{\gamma(t)}{\gamma_0}\right)^3 - 3\frac{\gamma(t)}{\gamma_0}\right) + ...\right) \quad (13)$$

$$\sigma''(t) = \gamma_0\omega\left(v_1(\omega,\gamma_0)\frac{\dot\gamma(t)}{\gamma_0\omega} + v_3(\omega,\gamma_0)\left(4\left(\frac{\dot\gamma(t)}{\gamma_0\omega}\right)^3 - 3\frac{\dot\gamma(t)}{\gamma_0\omega}\right) + ...\right) \quad (14)$$

which we wrote up to third order. We made use of $T_1(x) = x$ and $T_3(x) = 4x^3 - 3x$. Larger order expansions within the Chebyshev representation can be obtained from the tabulated polynomials.[74]

III. EXPERIMENTS

A. Sample Preparation. We briefly describe the model samples used here, the synthesis and the properties of which have been extensively described elsewhere.[20−24] The model filled elastomers consist of grafted silica particles dispersed in a poly(ethyl acrylate) matrix. Two kinds of grafter have been used: TPM (3-(trimethoxysilyl)propyl methacrylate), which can react with the monomer and thus create a covalent bond with the matrix (covalently grafted samples, CG), and C8TES (*n*-octyltriethoxysilane) with which there are only hydrogen bonds between the residual OH groups on the silica surface and the polymer (non-covalently grafted samples, NCG). Two samples are presented here: T50 CG 30% (silica diameter = 42 nm, grafting density = 3.2 nm^{-2}, silica volume fraction = 0.22) and T30 NCG 25% (silica diameter = 26 nm, grafting density = 2 nm^{-2}, silica volume fraction = 0.15).

B. Mechanical Measurements. The mechanical measurements were performed on an Anton Paar MCR 501 rheometer in simple shear strain with a plate−plate geometry. The samples were cylinders of 8 mm in diameter and 2 mm thick and were glued on the rheometer plates with a cyanoacrylate glue (Loctite 406). The measurements were done at 0.1 Hz and between 30°C (=T_g + 40 °C) and 80°C (=T_g + 90 °C). The rheometer was interfaced with a computer so that the strain and stress signals could be directly recorded and analyzed.

Contrary to the linear case, the generalized moduli depend on the strain and shear rate. The curves obtained by plotting σ' vs γ and σ'' vs $\dot\gamma(t)/\omega$ are thus not straight lines anymore. As an example, the signal analysis is shown in Figure 1 for the sample T30 NCG 25%. As explained in,[57] the inhomogeneity of the strain field in the plate−plate geometry has been taken into account. Indeed a correction factor of 3/2 has been applied to the experimentally measured nonlinear terms $e_3(\omega,\gamma_0)$ and $v_3(\omega,\gamma_0)$. This correction is applied in all following experimental results.

In order to describe the nonlinear behavior of the elastic part, we choose to use the slopes p_0, p_1, and p_2 in the σ' vs γ curve, as described in Figure 2:

- p_0 is the slope of the curve at small strain amplitude in the linear regime, it corresponds to $e_1(\omega,\gamma_0 = 0) = G'(\omega)$, which is the linear storage modulus,
- p_1 is the slope at the origin,
- p_2 is the slope at large strain.

Using this analysis, the ratios p_1/p_0 and p_2/p_0 can be plotted as a function of the strain amplitude. At small strain amplitudes, we expect both ratios to tend to 1, since in the linear case $p_2 = p_1 \to p_0$. At higher strains, it is observed that p_1 decreases and that $p_2 \geq p_1$ (Figure 2). As temperature decreases, the Payne effect is expected to increase, which is indeed what is observed in Figures 3a and 4a. The strain-hardening phenomenon, probed by the variation of p_2/p_0, seems to be less sensitive to temperature (see Figures 3b and 4b). Thus, the temperature dependence indicates that the variation of p_2 cannot be attributed to the strain-softening of glassy bridges only. The elastic stress is plotted as a function of the strain in Figure 5, at different temperatures, for a strain amplitude of 100%. The main result here is that strain hardening is observed, and that it is more pronounced at low temperature. Thus, in these samples and at these temperatures, the strain hardening cannot be explained only by the finite extensibility of the chains. The viscous stress as a function of the strain rate $\dot\gamma$ is also plotted in Figure 5 for the same temperatures. The higher harmonic contributions to the elastic stress are plotted in Figure 5.(c). Note that higher harmonic amplitudes are indeed small. We observed that e_3 is positive, which is the signature of the strain hardening behavior (see eqs 13 and 14).

IV. DESCRIPTION OF THE MODEL

We briefly recall the principle of the GBR model.[51]

A. Shift of the Glass Transition Temperature T_g in the Vicinity of the Fillers. It was proposed that the reinforcement is the consequence of an increase of the glass transition temperature of the matrix in the vicinity of the fillers.[37,39] In the GBRM, the fillers are modeled by solid spheres that interact with their neighbors through elastic springs that mimic the mechanical behavior of a glassy polymer layer. Indeed, the modification of the glass transition of a polymer domain is given by[23,51]

$$T_g(z,\sigma) \approx T_g\left(1 + \left(\frac{\beta}{z}\right)^{1/\nu}\right) - \frac{\sigma}{K} \approx T_g\left(1 + \frac{\beta}{z}\right) - \frac{\sigma}{K} \quad (15)$$

where z is the distance from the nearest filler interface, T_g is the bulk glass transition temperature of the pure rubber and $\nu \approx 0.88$. The first term in the right-hand side of eq 15 is the effect of the interaction between the fillers and the matrix.

dx.doi.org/10.1021/ma202278e | Macromolecules 2012, 45, 2891−2904

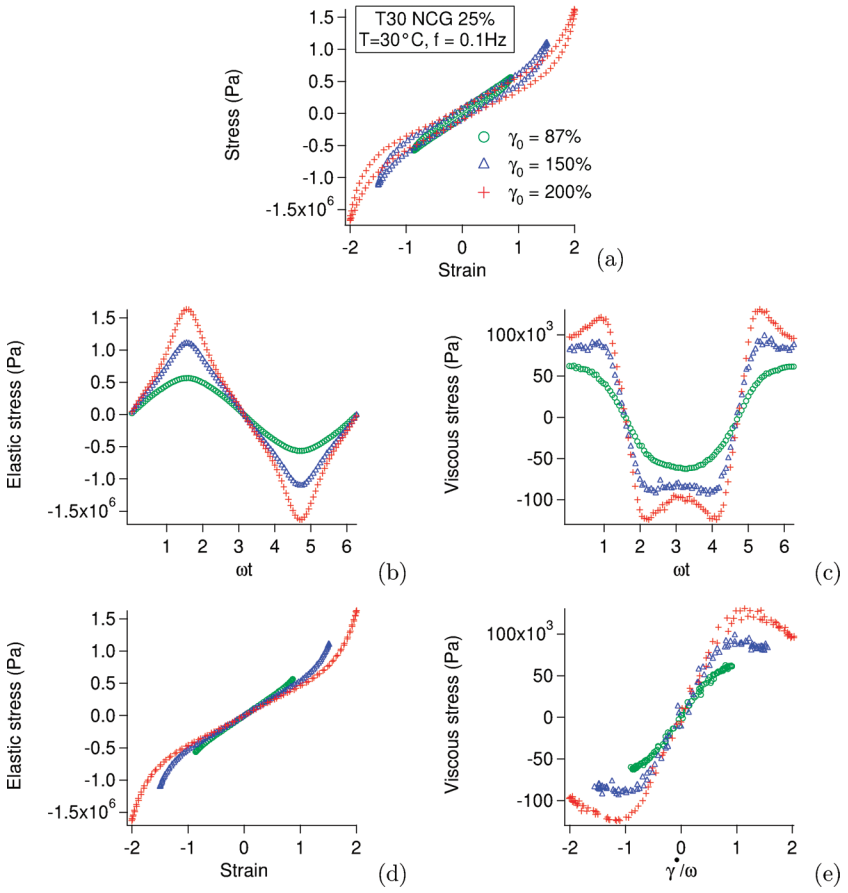

Figure 1. Signal analysis for the sample T30 NCG 25%. (a) Lissajous plot: stress vs strain. As the strain amplitude is increased, the Lissajous plot is more and more deviating from the elliptic shape obtained in the linear case. (b) Elastic stress (odd part of the total stress signal) vs time. (c) Viscous stress (even part of the total stress signal) vs time. (d) Elastic stress vs strain: the curve is not a straight line at large strain and shows a strain-hardening behavior. (e) Viscous stress vs $\dot{\gamma}(t)/\omega$: the nonlinearity is seen as a shear-thinning.

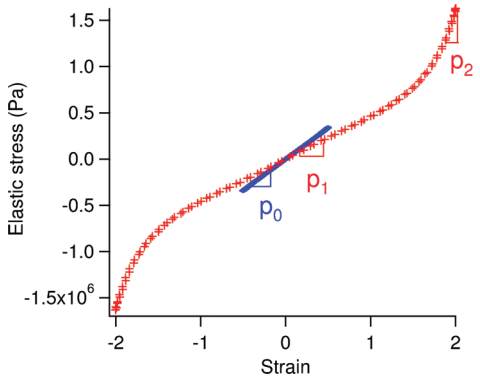

Figure 2. Elastic stress σ' as a function of the strain γ inside one strain cycle. p_0 is the slope of the curve at low strain amplitude, in the linear regime. p_1 and p_2 are the slopes in the nonlinear regime at small and large strain amplitudes, respectively.

The second term is the decrease of T_g due to the local stress σ, which is the plasticizing effect of an applied stress. K depends on the polymer. It relates the yield stress σ_y to the temperature T and the polymer glass transition temperature T_g by $\sigma_y = K(T_g - T)$. K is of the order of 10^6 Pa·K^{-1} typically.[66] β has dimension of a length, the precise value of which depends on the matrix–filler interaction. In the case of strong interactions, we argued in[51] that $\beta \sim 1$ nm.

B. Lifetime of Glassy Bridges: Aging. Glassy bridges are not permanent. Within a glassy bridge in between two neighboring particles, at equilibrium, we assume that the polymer locally has the dominant relaxation time τ_α given by the William–Landel–Ferry (WLF) law of the corresponding polymer,[67] modified by the T_g shift of eq 15 due to interfacial effects and the local stress σ. Hence under stress, glassy bridges may strain-soften when their local glass transition temperature decreases above the sample temperature. This temperature effect can also be expressed in term of time scale: we assume that the lifetimes (breaking times) of glassy bridges are comparable to the local dominant relaxation times τ_α of the glassy bridges. The breaking time is thus given by

$$\log\left(\frac{\tau_\alpha(z,\sigma)}{\tau_g}\right) = -\frac{C_1(T - T_g(z,\sigma))}{C_2 + (T - T_g(z,\sigma))} \quad (16)$$

where $T_g(z,\sigma)$ is given by eq 15 where z is taken to be half the distance between the surfaces of the neighboring particles, τ_g = 100 s (the relaxation time at T_g) and T is the temperature. C_1 and C_2 are the WLF parameters of the considered polymer.[67] Equation 16 gives *the equilibrium value of the breaking time*, which is obtained when the distance z, the local stress σ and the temperature T have been maintained fixed for a long time. In general, the breaking time depends on the history of the glassy bridge and is denoted by $\tau_\alpha(t)$. The corresponding evolution of glassy bridge is thus expected to follow the classical aging

dx.doi.org/10.1021/ma202278e | *Macromolecules* 2012, 45, 2891–2904

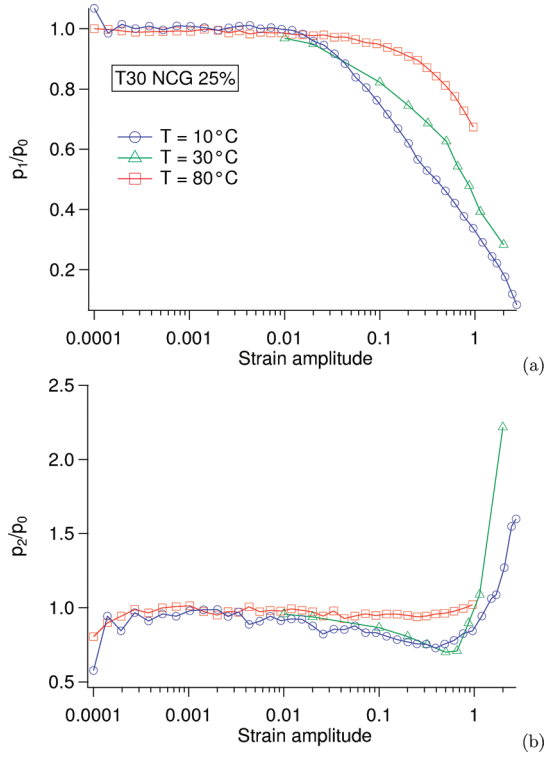

Figure 3. Ratios p_1/p_0 (a) and p_2/p_0 (b) vs strain amplitude at different temperatures (10, 30, and 80 °C) for the sample T30 NCG 25%. As temperature decreases, the Payne effect becomes larger so that p_1/p_0 decreases more abruptly. p_2/p_0 first follows this decrease and then increases due to the large strain-hardening.

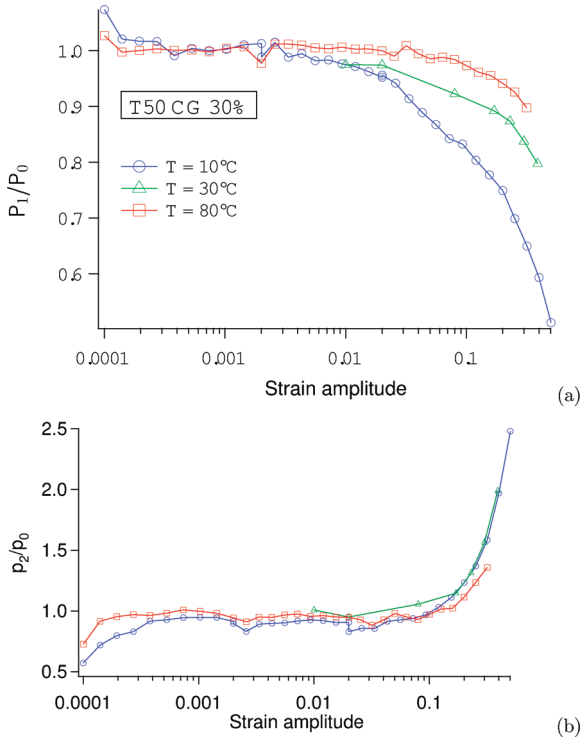

Figure 4. Ratios p_1/p_0 (a) and p_2/p_0 (b) vs strain amplitude at different temperatures (10, 30, and 80 °C) for the sample T50 CG 30%. Again the Payne effect is larger at lower temperature but it is smaller than for the T30 NCG 25% sample so that p_2/p_0 seems to be a monotonic increasing curve.

properites of glasses. $\tau_\alpha(t)$ evolves toward its equilibrium values linearly in time (see, e.g., ref 68).

It was shown that the kinetics of yield, birth and aging of glassy bridges is a key feature for explaining the dependence of $G'(\omega,\gamma_0)$ and $G''(\omega,\gamma_0)$ on the amplitude (Payne effect), and especially the presence of the peak of $G''(\omega,\gamma_0)$ at intermediate deformation amplitudes for strongly reinforced elastomers.[8,51] It is also essential for understanding the plastic behavior of filled elastomers.[50,52] As we shall see, this kinetics is also key for understanding the higher harmonic response of filled elastomers.

C. Modeling. The model described above needs to be solved numerically. The relevant degrees of freedom are the centers of mass of the fillers. The diameter d of the fillers sets the unit length scale. The dynamics is supposed to be non inertial. Each particle i interacts with $n = 10$ neighboring particles. The corresponding equation of motion for particle i is

$$\vec{F}_{\mathrm{el}}^{\,i} + \vec{F}_{\mathrm{hs}}^{\,i} + \vec{F}_{\mathrm{Hydro}}^{\,i} = \vec{0} \tag{17}$$

where $\vec{F}_{\mathrm{el}}$ is the elastic force between two neighboring particles and is the sum of the contributions of the glassy bridges and of the rubbery matrix. $\vec{F}_{\mathrm{hs}}$ is the hard core repulsion between fillers and $\vec{F}_{\mathrm{Hydro}}$ is the friction force between two neighboring particles. The elastic force is given by

$$\vec{F}_{\mathrm{el}}(\vec{r}) = -k_\infty(\vec{r} - l_0\vec{u}) - k_0(\vec{R}_{ij} - \vec{R}_{ij}^{\,ref}) \tag{18}$$

where l_0 is the equilibrium length of the rubbery springs, $\vec{r}$ is the vector joining the centers of the two particles, and $\vec{u}$ is the unit vector joining the two particles. To represent the effect of the rubbery matrix (of typical elastic modulus 1 MPa), we set $k_\infty = 1$. This spring constant sets the unit of modulus. All the results will therefore be expressed in units of MPa. The glassy modulus, 10^9 Pa, is typically 3 orders of magnitude larger than the rubbery modulus. The glassy spring constant is thus set to $k_0 \sim 10-100$. (Note that k_0 is much smaller than 1000 because geometrical aspects regarding glassy bridges have to be taken into account[51]). Finally, $\vec{R}_{ij} = \vec{R}_i - \vec{R}_j$, and $\vec{R}_i$ is the vector position of filler i. A viscous force between two neighboring particles in our simulations has to be added to stabilize the simulation, and is written as

$$\vec{F}_{\mathrm{Hydro}} = -\zeta\frac{\mathrm{d}\vec{R}_{ij}}{\mathrm{d}t} \tag{19}$$

The relaxation time of glassy bridges then follows a linear evolution in time toward its equilibrium value. More details regarding the implementation of the model into a numerical code are given in refs 69−71. In ref 51, we discussed in more detail how the physical parameters of the system can be translated into the parameters of the simulation. The length scales are made dimensionless thanks to the filler diameter which set the unit length scale. If we assume that their diameter is 20 nm, typical dimensionless values for β will be of order 0.05 (corresponding to $\beta = 1$ nm in physical units). The parameters and the corresponding values used in our simulations are summarized in Table 1.

V. SIMULATIONS: RESULTS

We have considered a system of 5000 particles with a volume fraction $\Phi = 40\%$. To describe the dynamics of the glassy springs, the WLF parameters of polyisoprene (PI),[72] for which $T_g = 213$ K, have been used. The parameter K, which describes

dx.doi.org/10.1021/ma202278e | Macromolecules 2012, 45, 2891−2904

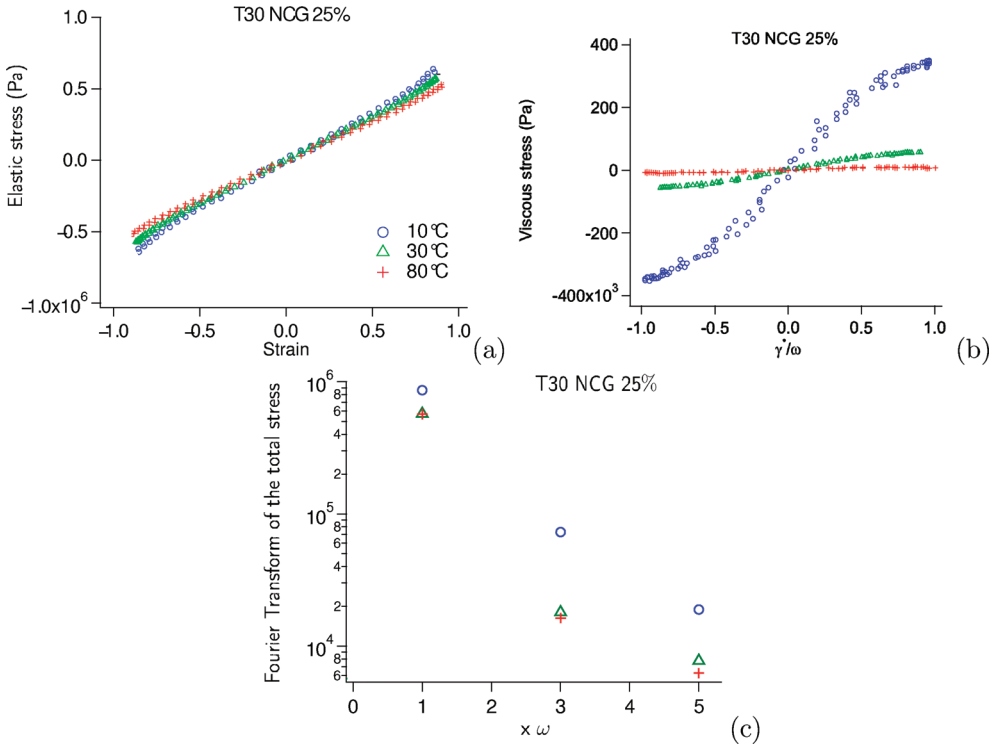

Figure 5. Signal analysis for the sample T30 NCG 25%. (a) Elastic stress (odd part of the total stress signal) vs strain $\gamma(t)$, for the same deformation amplitude γ_0 at three different temperatures. One observes significant strain hardening at low temperature. (b) Viscous stress (even part of the total stress signal) vs $\dot{\gamma}(t)/\omega$ for the same experiments. (c) Components $\gamma_0 e_n(\omega,\gamma_0)$ of the Chebyschev expansion of the total stress in the same experiments, up to the fifth harmonic. Though small, we can note that the stronger the reinforcement (i.e., the lower the temperature), the stronger the higher harmonic contribution.

Table 1. Parameters of the Model[a]

parameter	physical value	value in the simulation
number of particles		N = 5000
volume fraction	10−40%	40%
filler diameters	20 nm	d = 1.0
connectivity of springs		n = 10
rubbery modulus	5 × 10^5 Pa	k_∞ = 1
glassy modulus	10^9 Pa	k_0 = 10−100
glass transition temperature T_g of the pure rubber	213 K	T_g = 213 K
temperature of the experiment T	T	T = 263 K
typical deformation rate	1 s^{-1}	$\dot{\gamma}$ = 1 s^{-1}
dissipative modulus at large deformation amplitudes	10^6 Pa	ζ= 4 s
coefficient β	0.4−0.8 nm	0.02−0.04
coefficient K	10^6 Pa·K^{-1}	0.3
coefficient α	$\lesssim$1	0.4

[a]In addition to the glass transition temperature of the matrix, one needs the complete WLF law of the considered polymer.

the stress-softening in eq 15, has been taken to be 0.3 MPa·K^{-1}. The other parameters characterizing the network of soft springs and the hardcore interactions between particles are the same as in our previous studies and are fixed.[50,51] We have considered two values of the dimensionless parameter β, 0.04 and 0.02, and two values for the parameter k_0, 10 and 100. For each value of β and k_0, simulations have been performed at various temperatures, from T = 263 K = T_g + 50 K up to T = 323 K = T_g + 110 K. A sinusoidal deformation $\gamma(t) = \gamma_0 \sin(\omega t)$ with a fixed pulsation ω = 1 s^{-1} has been imposed. As the model system may be more dissipative than the experimental systems because of the large value of the friction ζ, the viscous contribution on the total stress $\sigma_{hydro}(t) = G''_{\text{high T}}\,\gamma_0 \cos(\omega t)$, where $G''_{\text{high T}} \simeq$ 3.86 MPa is the loss modulus measured at high temperature for the smallest value of β (T = 323 K, β = 0.02), has been subtracted from the stress. Note in particular that, for these parameter values, the apparent modulus is found to be independent of the strain amplitude (i.e., there is no Payne effect), and so that, in this regime, the viscous stress originates only from the friction coefficient ζ between particles.

The elastic response of a sample defined by the parameters β = 0.04 and T = 323 K is shown in Figure 6. Both the stress versus strain curves, the elastic and viscous stresses as a function of time and the elastic and viscous stresses as a function of strain and strain rate, respectively, are shown. A strain-hardening behavior is observed. The parameters chosen here correspond to a moderate reinforcement, and a relatively high temperature. The main features observed in the experiments (Figure 1) are reproduced qualitatively. In particular, the elastic curve shows strain-hardening at large amplitude, and the viscous stress depends nonmonotonously on the instantaneous strain rate.

The elastic stress at several temperatures and for two different values of β, 0.02 and 0.04, is plotted as a function of strain in Figure 7. The corresponding viscous stress (for β = 0.02 only) is plotted in Figure 8. A hardening of the elastic stress is observed at the extremities of the cycle. The stronger the reinforcement, and the lower the temperature, the larger the hardening effect. The observed behavior is also qualitatively similar to that observed experimentally in Figure 5 where strain hardening was found to be significant at low temperature. Regarding the viscous stress, a behavior qualitatively similar to

dx.doi.org/10.1021/ma202278e | Macromolecules 2012, 45, 2891−2904

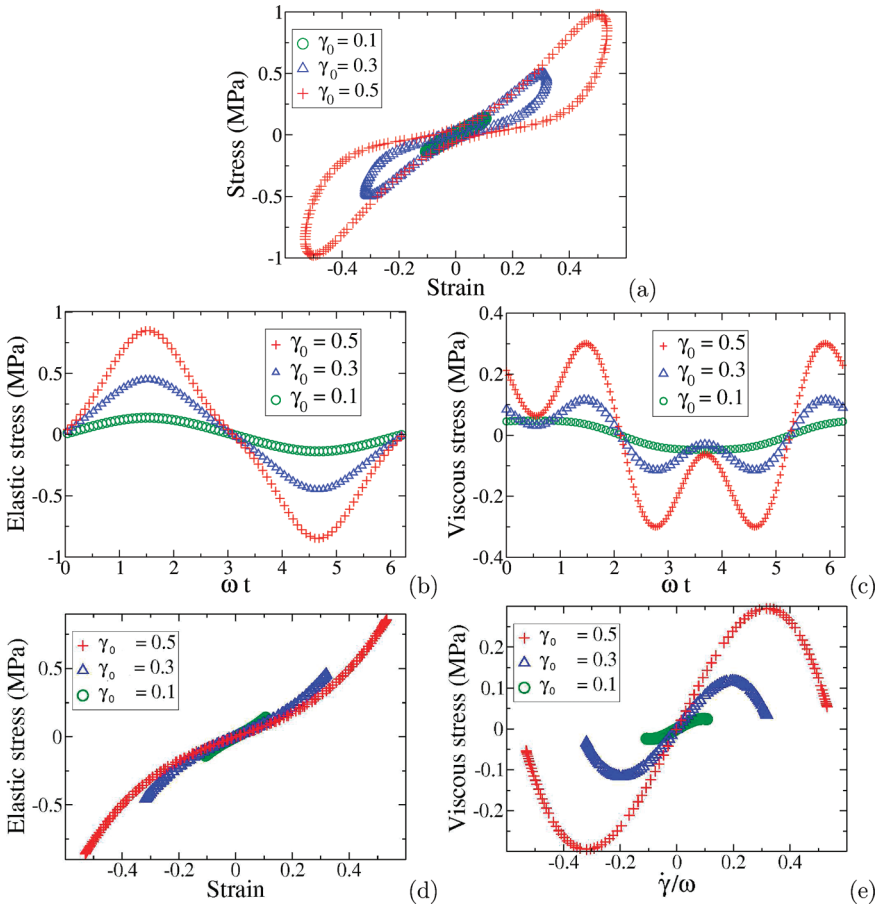

Figure 6. Stress curves simulated with the model with $\beta = 0.04$, $k_0 = 100$ and $T = 323$ K (using the WLF parameters of PI with $T_g = 213$ K). Other parameters are $\Phi = 40\%$; $K = 0.3$; $\zeta = 4$ s; pulsation $\omega = 1$ s^{-1}. The contribution to the stress due to the friction between particles has been subtracted as explained in the text. (a) Lissajous plot: stress vs strain. (b) Elastic stress vs time. (c) Viscous stress vs time. (d) Elastic stress vs strain: the curve at large amplitude shows strain-hardening. (e) Viscous stress vs $\dot{\gamma}(t)/\omega$: the nonlinearity is seen as a shear thinning. The observed behavior is qualitatively similar to the experimental results of Figure 1.

that of the experimental data, in which the viscous stress goes through a maximum at intermediate strain rates, is observed.

VI. DISCUSSION

A. Aging or Rebirth of Glassy Bridges within a Strain Cycle. First let us recall that the decrease of the elastic modulus can be interpreted as a strain softening of the glassy bridges as observed experimentally in ref 22 and in the frame of the GBRM.[51] Thus, the decrease, with the strain amplitude γ_0, of the slope of $\sigma'(\gamma)$ at zero strain from p_0 to p_1 can be interpreted as a decrease of the average number of glassy bridges in the systems with the average level of stress. We will show now that we can interpret the strain hardening as the consequence of the slowing down of the strain rate at the extremities of the cycle. We focus on the aging—or rebirth—of glassy bridges within a strain cycle. The slower the strain rate, the more glassy bridges can recover relatively long relaxation times. These recoveries occur most efficiently in the parts of the cycle where the strain rate is the smallest. As a consequence, these glassy bridges that rebuild during the slowest part of the strain cycle will contribute to the elastic response. This effect appears explicitly in the GBRM. Let us define the integrated distribution of relaxation times $P(\log \tau)$ as the number of glassy springs having a relaxation time larger than, or equal to τ. $P(\log \tau)$ is related to the distribution of relaxation times by the relation

$$P(\log \tau) = N_{tot} \int_{\tau}^{\infty} Q(\tau)\, d\tau \tag{20}$$

where $Q(\tau)$ is the normalized distribution of relaxation times, and N_{tot} is the total number of glassy springs. In our simulations, this total number is constant and equal to $N_{tot} \approx 25000$. This number corresponds to the fact that our system contains 5000 beads, which interact typically with 10 neighbors. Thus, the number of glassy bridges is fixed, only the relaxation time associated with each glassy bridge varies during the simulations. The integrated distribution is thus related also to the distribution by the relation $N_{tot}Q(\tau) = (-1/\tau)\ (dP(\log \tau))/(d[\log(\tau)])$. $P(\log \tau)$ is therefore a decreasing function of $\log\tau$, from N_{tot} down to zero at large values of $\log\tau$ as can be seen in Figures 9 and 10. Large values of the slope of P correspond to peaks in the distribution Q. Note that the sharp drop at $\log \tau \approx -2$ corresponds to the short time cutoff in our simulations which we set at 10^{-2} s and is thus an artifact of the simulation. We assume thus that the relaxation time of glassy bridges can never be shorter than 10^{-2} s, which is not important because the considered frequencies in the simulations are always much smaller than 100 Hz. In Figure 9, the integrated distribution $P(\log \tau)$ in systems undergoing a sinusoidal deformation of amplitude $\gamma_0 = 0.5$ is plotted at different instantaneous values of

dx.doi.org/10.1021/ma202278e | Macromolecules 2012, 45, 2891−2904

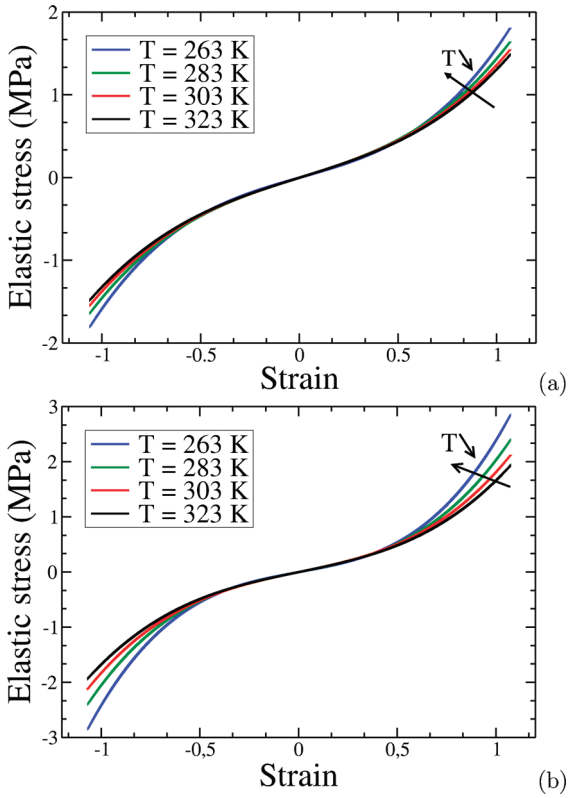

Figure 7. Simulations: elastic stress as a function of strain at different temperatures. The parameters are $\beta = 0.02$, $k_0 = 100$ (a) and $\beta = 0.04$, $k_0 = 100$ (b). A temperature dependent hardening is observed at the extremities of the cycle, due to a slowing down of the deformation rate. The stronger the reinforcement, and the lower the temperature, the larger the effect.

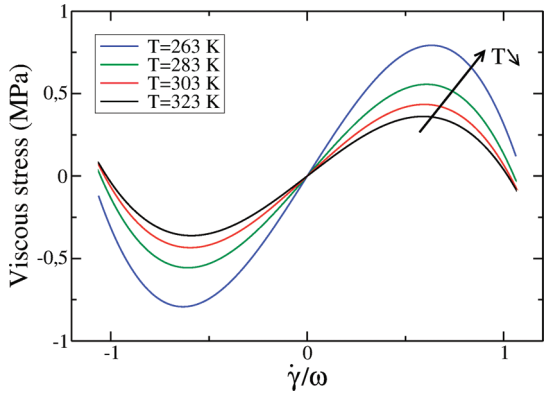

Figure 8. Simulations: viscous stress in a sample with $\beta = 0.02$, $k_0 = 100$, $\gamma_0 = 100\%$, at different temperatures.

the strain $\gamma(t)$. We consider a relatively strongly reinforced system ($\beta = 0.04$; $T = 263$ K), and the same system at higher temperature ($T = 323$ K). Indeed, one can see in Figure 9 that the number of glassy bridges with breaking times larger than typically 1 s—the solicitation period—is larger for values of $\gamma(t)$ close to the maximum $\gamma_0 = 0.5$. When the strain rate slows down, the relaxation time of the glassy bridges can increase, whereas at high values of the strain rate the glassy bridges break more frequently. This is the same mechanism as the one we discussed in ref 50 for accounting for the unique plastic properties of filled elastomers. Indeed, it was argued in ref 50

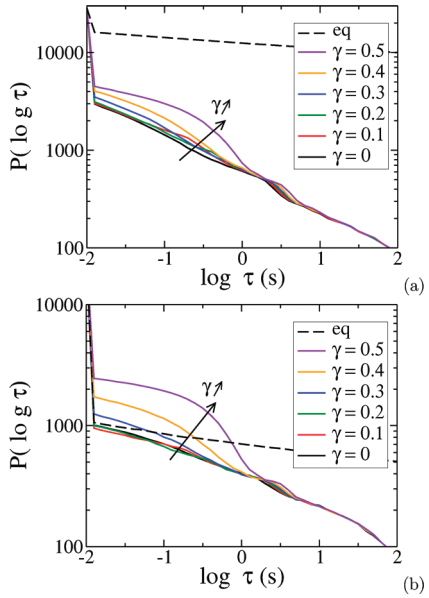

Figure 9. Integrated distributions of relaxation times of glassy bridges $P(\log\tau)$ of systems undergoing a sinusoidal deformation with an amplitude $\gamma_0 = 0.5$, plotted at different values of the instantaneous strain $\gamma(t)$:from bottom to top, $\gamma = 0$; 0.1; 0.2; 0.3; 0.4 and γ_{max}. $P(\log \tau)$ is the number of glassy springs having a relaxation time larger than τ. The total number of glassy bridges is ≃25000. (a) reinforced system ($\beta = 0.04$; $T = 263$ K), for which p_2 is smaller than p_0 (see Figure 11); (b) a moderately reinforced system ($\beta = 0.04$; $T = 323$ K) for which p_2 is larger than p_0 (see Figure 11). Other parameters are the same as in Figure 6. Dashed curves show the distributions prior to deformation. In the moderately reinforced system (b), the number of glassy springs having a lifetime comparable at least to the deformation period, $\tau \sim 1$ s, may be larger than at equilibrium. In this case, the slope p_2 is larger than p_0.

that when a static strain is applied and maintained constant for a long time, the glassy bridges recover long relaxation times in this new imposed deformation state, thus creating a new reference state corresponding to a plastic deformation with respect to the initial state at rest (before the static strain has been applied). The same mechanism is at work in the case of cyclic strain discussed in this paper. The observed hardening is a consequence of the aging of the glassy bridges at the extremities of the deformation cycles: thus this does not correspond to strain hardening *per se*, but to what we propose to call "slowing down hardening", a property which should be observed in self-healing systems in general.

The mechanisms at work are schematized in Figure 10, in order to make the interpretation we propose more precise. In Figure 10a, we represent the state of the sample before deformation are applied, and after a long aging time which has allowed the glassy bridges to age up to time scales comparable to 10^5 s. It corresponds to the integrated distribution of relaxation times in thick dashed line (Figure 10d). When a periodic deformation of relatively large amplitude γ_0—e.g., 50% or 100%—is applied, and after a few cycles when the permanent regime is reached, many glassy bridges of long relaxation times have melted (Figure 10b). The distribution of relaxation times is modified (thick black line in Figure 10d). Glassy bridges with very long relaxation times are still present in the system, but they form isolated clusters which are not submitted fully to the large deformation amplitude applied on a macroscopic scale. These clusters are separated by polymers which is in a rubbery state,

dx.doi.org/10.1021/ma202278e | *Macromolecules* 2012, 45, 2891–2904

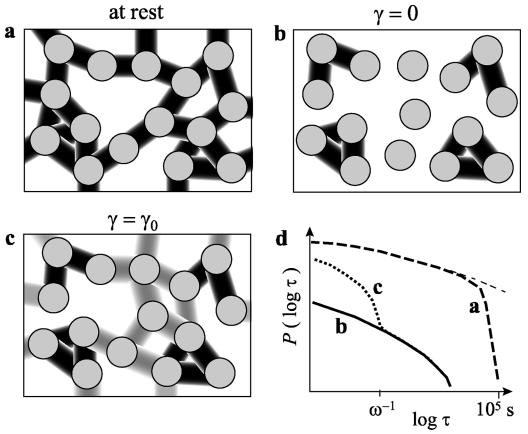

Figure 10. Schematics of the glassy bridges in a filled elastomer. In black, we represent the glassy bridges with very long relaxation times, i.e., much longer than the solicitation period ω^{-1}. In gray, these are glassy bridges with lifetimes comparable to the deformation period. In white, we represent either the rubbery matrix, or glassy bridges with lifetimes much shorter than ω^{-1}. See the text for comments. (a) Glassy bridges in an aged sample, e.g. with an aging time of order 10^5 s, before any deformation is applied. (b) Snapshot of the glassy bridges in the same sample when submitted to a periodic deformation of large amplitude. This snapshot is taken at a time which corresponds to a maximum of the shear rate, i.e., when the instantaneous value of the strain amplitude γ is zero. (c) Snapshot of the glassy bridges, as in part b, but taken at an extremity of the deformation cycle, i.e., at $\gamma = \gamma_0$. Because the strain rate slows down in the vicinity of an extremity of the cycle, glassy bridges with a slightly larger relaxation times have time to appear as compared to b). (d) Integrated distribution of relaxation times corresponding to cases a (dashed curve), b (full curve), and c (dotted curve). The thin dashed curve corresponds to the integrated distribution at equilibrium, which may not be reached in an accessible aging time.

or close to that state. Within one cycle, however, in the part of the cycle for which $\dot{\gamma}$ is small, the relaxation times of the glassy bridges linking such clusters increase, and come close to the value ω^{-1}. That corresponds to the glassy bridges in light gray in Figure 10.c. This is the origin of the slowing down hardening. During the permanent regime of the applied periodic solicitation, the distribution of relaxation time oscillate between the behavior described in Figure 10, parts b and Figure c, corresponding to the dotted line and the thick black line in Figure 10d, respectively.

B. Effect on the Elastic Stress. Let us focus now on the nonlinear elastic stress. The ratios p_1/p_0 and p_2/p_0 are plotted as a function of the strain amplitude in Figures 11 and 12, at different temperatures and for the same parameter values as in Figure 7. For the two interaction parameters β considered, the ratio p_1/p_0 decreases more abruptly, i.e., the Payne effect becomes larger, when temperature decreases. For the system with a weak polymer/filler interaction, Figure 12 shows that at high temperature, the Payne effect is modest and practically independent of temperature in the considered temperature range. For the relatively reinforced system $\beta = 0.04$, the ratio p_2/p_0 decreases with the strain amplitude at low temperature, while it increases at high temperature. On the other hand when $\beta = 0.02$, for all the temperatures considered, the ratio p_2/p_0 increases with the strain amplitude, following a curve that is nearly independent of temperature, except for the lowest considered temperature ($T = 263$ K).

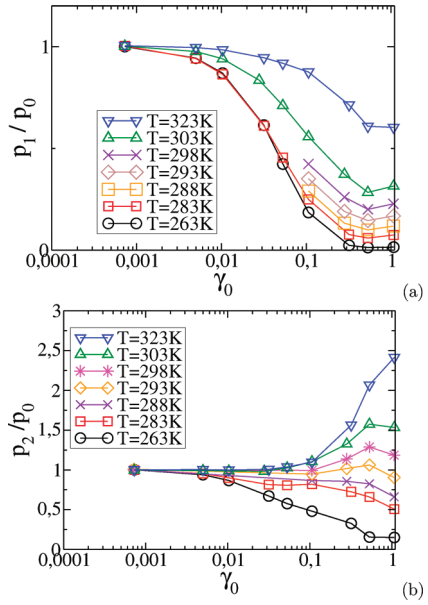

Figure 11. Simulation results: the ratios p_1/p_0 (a) and p_2/p_0 (b) vs strain amplitude γ_0 at different temperatures (T = 263 K, 283 K, 303 and 323 K) for $\beta = 0.04$ and $k_0 = 100$. As temperature decreases, the Payne effect becomes larger so that p_1/p_0 decreases more abruptly. p_2/p_0 decreases with the strain amplitude at low temperature, while it increases at high temperature. Other parameters are the same as in Figure 6. The results are to be compared to those of Figure 3.

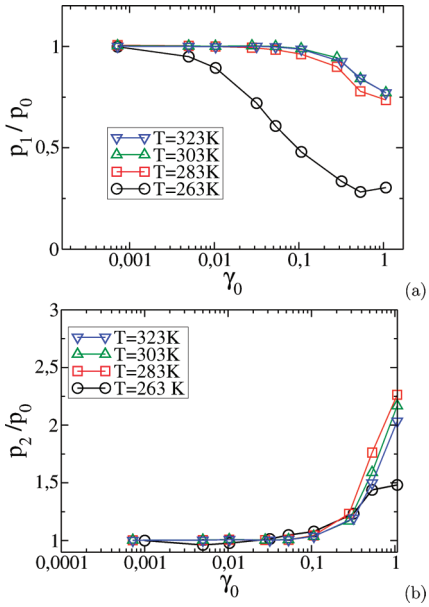

Figure 12. Simulation results: the ratios p_1/p_0 (a) and p_2/p_0 (b) vs strain amplitude at different temperatures (T = 263 K, 283 K, 303 and 323 K) for a small value of $\beta = 0.02$ and $k_0 = 100$. At high temperature, the Payne effect is modest and practically independent of temperature. At all considered temperatures, the ratio p_2/p_0 increases with the strain amplitude, following a curve which is nearly independent of temperature. Other parameters are the same as in Figure 6. The results are to be compared to those of Figure 4.

We have proposed above that the elastic modulus at the extremities of the strain cycle $\gamma(t) = \gamma_0$ can be larger than that at $\gamma(t) = 0$ (for a given deformation amplitude γ_0) because glassy bridges can build relatively long relaxation times around

dx.doi.org/10.1021/ma202278e | Macromolecules 2012, 45, 2891−2904

positions for which $\dot{\gamma} = 0$. On the other hand, one might expect that the elastic modulus should be smaller than p_0 there. This is the case for strongly reinforced systems, with large Payne effect: the "slowing down hardening" cannot compensate for the strong amplitude of the Payne effect, as can be seen in Figure 11 for a system with $\beta = 0.04$ at $T = 263$ K. On the other hand, for moderately reinforced systems (the system with $\beta = 0.04$ considered in Figure 11 at high temperature, i.e., T = 303 or 323 K, and the system with $\beta = 0.02$ in Figure 12 at any temperature), the slope p_2 is larger than p_0, as it is also the case experimentally (see Figures 3 and 4). We propose the following explanation: the applied deformation changes the distribution of distances between fillers, and can bring some of them closer together. This results in a shift of glassy bridge lifetimes toward longer times and thus possibly in a stiffening of the sample at large deformation amplitudes as compared to the undeformed state. This interpretation is consistent with Figure 13 which displays the distributions of distances $N(z)$ between the centers of mass of neighboring particles at different instantaneous values of the strain. The results for a relatively strongly reinforced sample ($\beta = 0.04$ and $T = 263$ K) are plotted in Figure 13a. No shift toward smaller distances is observed in this case.

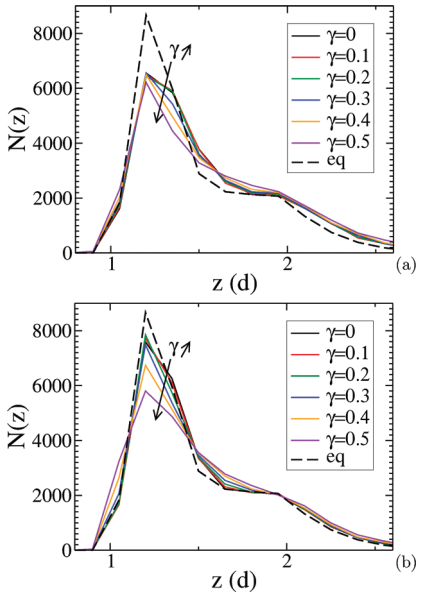

Figure 13. Distribution of distances $N(z)$ between the centers of mass of neighboring particles for systems undergoing a sinusoidal deformation of amplitude $\gamma_{max} = 0.5$, plotted at different values of the instantaneous strain: from top to bottom, $\gamma = 0$, 0.1, 0.2, 0.3, and 0.4 and γ_{max}. $N(z)$ is the number of pairs whose center of mass lies between z and $z + \Delta z$, with $\Delta z = 0.15d$. The total number of distinct pairs of particles is ≃25000. Key: (a) reinforced system ($\beta = 0.04$; $T = 263$ K); (b) a moderately reinforced system ($\beta = 0.04$; $T = 323$ K). Other parameters are the same as in Figure 6. Dashed curves show the equilibrium distributions prior to deformation. Note that at 323 K and at maximum strain, two neighboring particles may come very close to each other, consistently with the large value of p_2 compared to p_0.

In the case of a moderately reinforced system ($\beta = 0.04$ and $T = 323$ K, Figure 13b), it is observed that some fillers can come closer together under applied strain as compared to the equilibrium system, thus leading to a stiffening at large deformation amplitudes. The difference regarding the distribution of distances between the initial, nondeformed system, and the one at the maximum deformation amplitude might seem tiny. However, one must bear in mind that the reinforcement parameter β is not very large ($\beta = 0.04$), and that the temperature is relatively high ($T = 323$ K). The glassy layer thickness e_g, given by[21,22]

$$e_g = \beta \frac{T_g}{T - T_g} \tag{21}$$

is on the order of 0.09 in the dimensionless system of the simulations, which corresponds to about 2 nm in real samples. As a consequence, the polymer layers situated between fillers further apart than $z \approx 1.2$ are more than 60 K above their glass transition, and do not contribute to the building of glassy bridges. Only fillers closer than $z \approx 1.2-1.1$ contribute significantly to the reinforcement. We see thus that the elastic forces within the material can bring some fillers closer together as compared to the initial nondeformed sample, and lead to values of p_2 larger than p_0.

C. Effect on the Dissipative Stress. As discussed in ref 51, the dissipation in filled elastomers has three different origins. The most obvious is the one of the elastomer matrix, far from the polymer−filler interfaces. The second one is due to the transition region between the matrix and the glassy layer. The third one is due to the kinetics of rupture and rebirth of glassy bridges, which is of interest here. This third source of dissipation becomes efficient at intermediate deformation amplitudes γ_0. Indeed, at small γ_0, the lifetime distribution of the glassy bridges is not modified by the deformation and the second origin of viscous stress dominates. However, at intermediate to large values of γ_0 the kinetics of rupture and rebirth of glassy bridges may contribute significantly to the dissipation. More precisely, the peak observed both in the experiments and in the simulations (see Figures 1 and 6, respectively) may also be explained by the "slowing down hardening". Let us consider the behavior of the viscous stress as a function of $\dot{\gamma}$. At the point at which $\dot{\gamma} = 0$, the viscous stress is zero. Close to this point, the lifetimes of the glassy bridges are comparatively large, because of the "slowing down hardening" effect discussed above. Then, $\dot{\gamma}$ increases and $\sigma''(t)$ first increases linearly (as can be seen in Figures 1 and 6), because the distribution of glassy bridge lifetimes is not yet modified as compared to the situation at zero shear rate. As the strain rate, as well as the instantaneous strain, increase further, the distribution shifts to shorter times, as it is observed in Figure 9. The sample then becomes less dissipative, which corresponds to the peak of $\sigma''(t)$.

D. Nonlinearity and Nonharmonic Behavior. To further illustrate how the nonlinear behavior depends on the reinforcement parameters k_0, β and T, the stress/strain curve, the elastic stress as a function of the strain and the viscous stress as a function of the strain rate are shown for a system with $\beta = 0.04$ and $k_0 = 10$ at $T = 323$ K (Figure 14) and for a system with $\beta = 0.02$, $k_0 = 100$, $T = 263$ K (Figure 15). In this latter case, the cubic contribution to the viscous strain dominates at large strain rates. In some instances the viscous stress may show values of opposite sign to the strain rate for large values of the latter, as it is observed in Figure 8. The contributions of the harmonics ω, 3ω and 5ω to the elastic stress are plotted in Figure 16. It is observed that $\gamma_0 e_5(\omega,\gamma_0)$ is about one decade smaller than $\gamma_0 e_3(\omega,\gamma_0)$, which is itself one decade smaller than $\gamma_0 e_1(\omega,\gamma_0)$, as it is the case regarding experimental results (see Figure 5c). The stronger the reinforcement, i.e., the lower the temperature in Figure 16, the larger the amplitude of $e_3(\omega,\gamma_0)$ and $e_5(\omega,\gamma_0)$.

dx.doi.org/10.1021/ma202278e | Macromolecules 2012, 45, 2891−2904

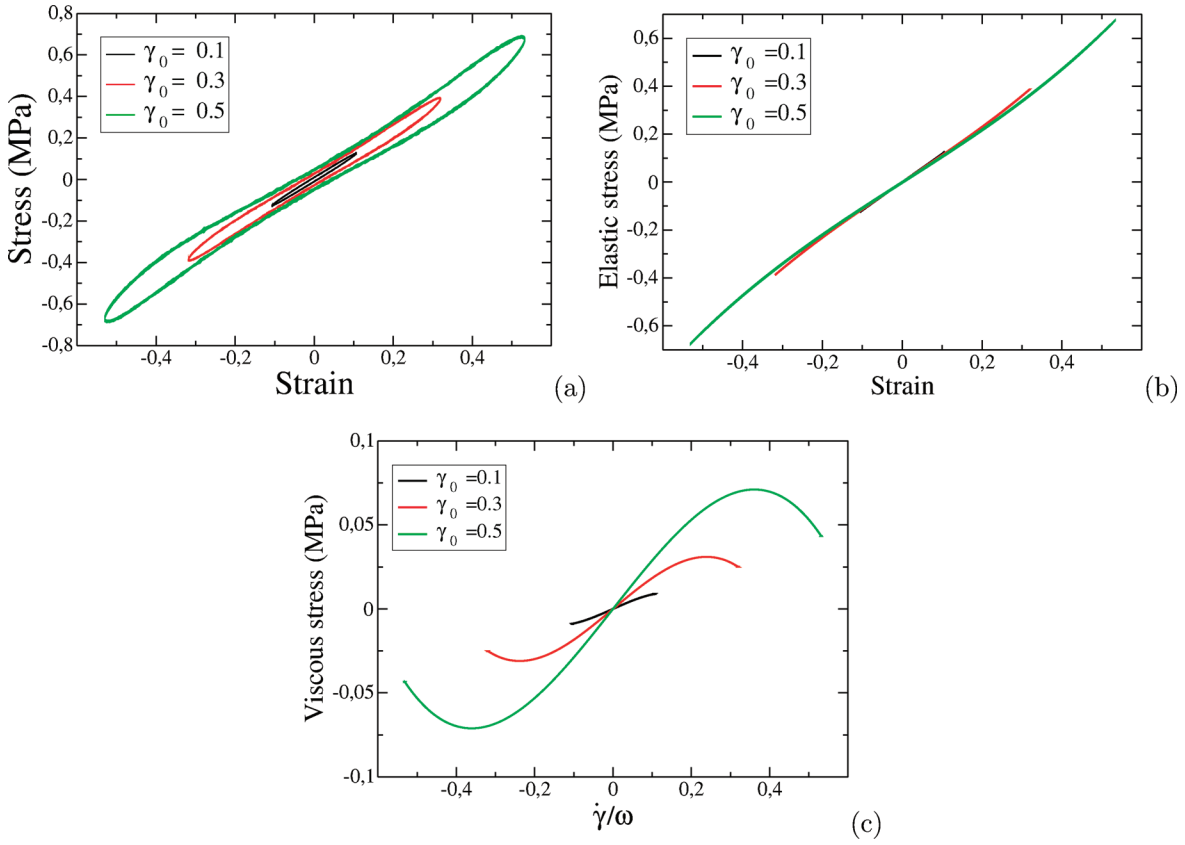

Figure 14. Simulations: stress/strain curve (a), elastic stress (b), and viscous stress (c) of a sample with β = 0.04, k = 10, and T = 323 K.

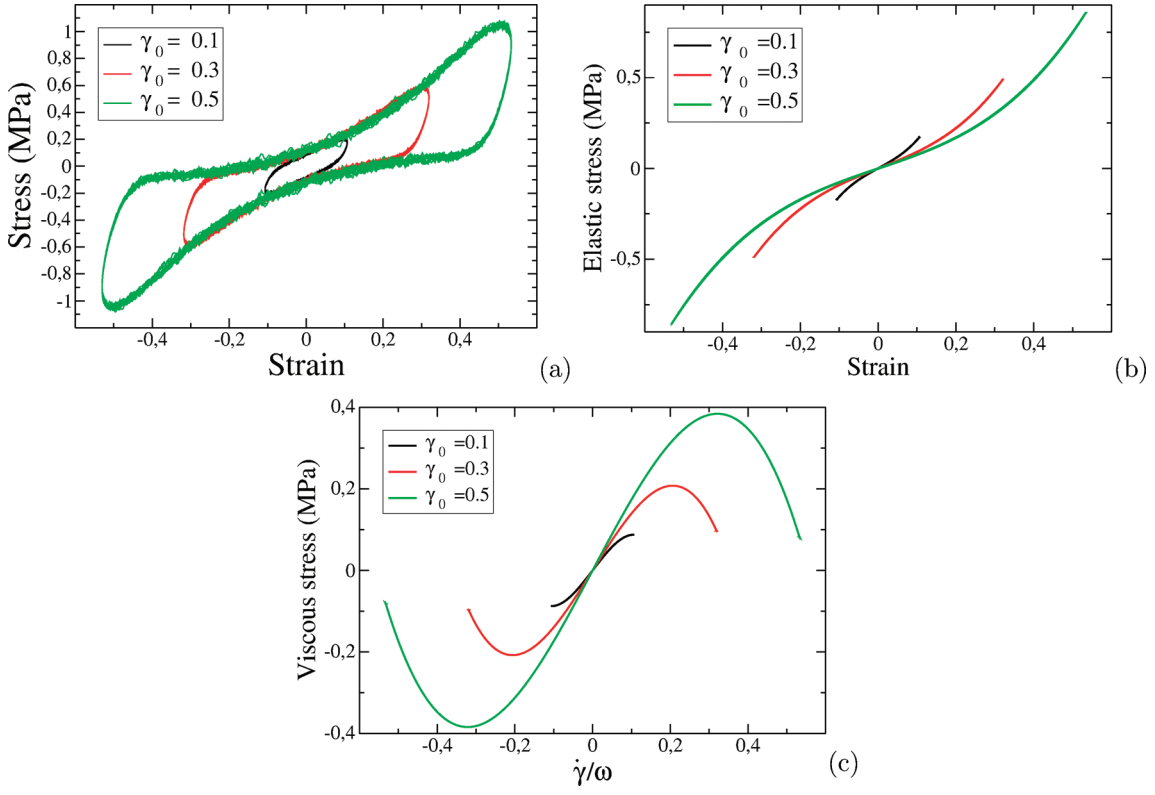

Figure 15. Simulations: stress/strain curve (a), elastic stress (b), and viscous stress (c) of a sample with β = 0.02, k = 100, and T = 263 K.

Thus, the "slowing down hardening" is mainly due to the contribution of the third harmonics. On the other hand, e_3 is quite small compared to the apparent "slowing down hardening" observed in Figure 5a. The hardening is defined by the slope

dx.doi.org/10.1021/ma202278e | *Macromolecules* 2012, 45, 2891–2904

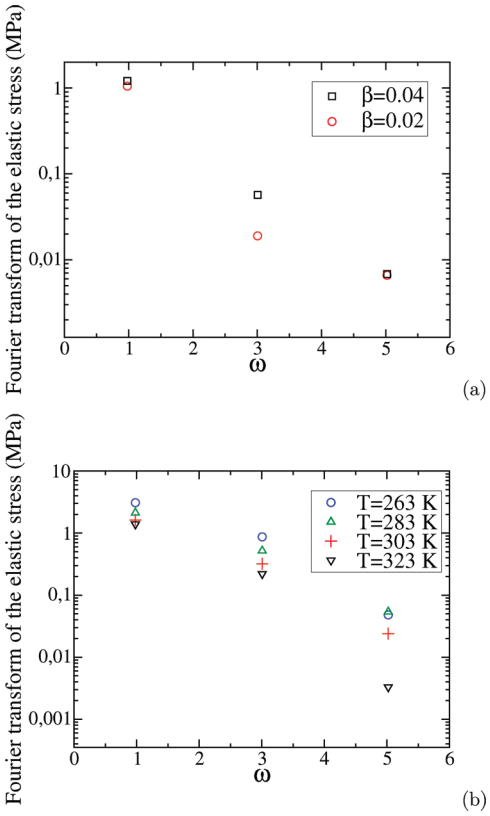

Figure 16. Components of the Chebyschev expansion of the total stress $\gamma_0 e_n(\omega,\gamma_0)$, up to the fifth order for systems deformed with an amplitude $\gamma_0 = 0.5$. (a) $k_0 = 100$, $T = 323$ K; (b) $k_0 = 10$, $\beta = 0.04$. The data in part a with $\beta = 0.02$ are qualitatively very similar to the experimental results displayed in Figure 5c, especially those at 80 °C. Note also that the stronger the reinforcement, the larger the amplitude of higher harmonics.

(or differential modulus, as it is often called[75]) at large strain $P_2 = ((d\sigma'(t))/(d\gamma))|_{\gamma=\gamma 0}$. According to eqs 7 and 9:[74,76]

$$p_2 = \frac{d\sigma'}{d\gamma}|_{\gamma=\gamma_0} = \sum_{n:\text{odd}}^{\infty} n^2 e_n \tag{22}$$

That is, up to third order

$$p_2 = \frac{d\sigma'}{d\gamma}|_{\gamma=\gamma_0} \approx e_1 + 9e_3 \tag{23}$$

which could be deduced directly from eq 13 as well. Thus, even if e_3 is small as compared to e_1, it can lead to a significant hardening because of the factor 9 in this equation, which was also noted in ref 61.

A last point that deserves to be discussed regards the specific features of the nonlinear behavior of filled elastomers. As mentioned in the introduction, it is often thought that a nonlinear behavior under periodic solicitations at frequency ω should necessarily result in the appearance of contributions to higher frequency harmonics 3ω, 5ω, ..., which is the case in particular when the stress is a nonlinear, nonretarded function of the deformation x with a constitutive relation of the type: $\sigma(x) = k^{(1)}x + k^{(3)}x^3 + k^{(5)}x^5 + ...$ Under these circumstances, large higher harmonic contributions are indeed associated with a strongly nonlinear behavior. On the contrary, as we have discussed, it is well-known that filled elastomers have a strong nonlinear behavior, in the sense that the elastic modulus $G'(\gamma_0,\omega) = e_1(\gamma_0,\omega)$ strongly depends on γ_0—which is the Payne effect—whereas higher harmonics are quite small, as we have seen both in experimental results and in simulations. Filled elastomers thus behave as nonlinear materials as regards their response to deformation of increasing amplitudes, but as almost linear materials under permanent oscillatory shear of fixed amplitude. The deformation amplitude γ_0 essentially modifies the lifetime distribution of glassy-bridges, and thus their contribution to the mechanical response. In particular, for deformation amplitudes larger than a few percent, or ten percents, depending on the systems, the difference between the initial distribution of relaxation times and the distribution during the experiment is huge (see Figure 9). On the other hand, the variation of the distribution of relaxation times in one strain cycle can be quite small as shown in the same figure. In a first approximation, the applied periodic deformation modifies the *average* distribution of relaxation times. If this distribution did remain constant—and thus equal to its average value—during the sinusoidal strain cycles, the response would be rigorously harmonic. However, as we have discussed, the lifetimes of glassy bridges evolve slightly during the deformation cycle, which results in small higher harmonic contributions.

VII. CONCLUSION

We have shown that the GBRM can account for the nonlinear behavior of filled elastomers submitted to large amplitude oscillatory shear experiments. Though they might be present in some experiments, and certainly at sufficiently large deformation amplitudes, the finite extensibility of the chains did not dominate the non sinusoidal response of the studied samples. Our point of view is that filled elastomers can be described by two elastic moduli: a rubbery one, and a glassy one, and the distribution of relaxation times associated with the glassy component. The applied strain does not change the elastic moduli, but modifies the lifetime distribution and thus, in particular, modifies the contribution of the glassy modulus. Thus, the main feature of the nonlinear response during periodic oscillations is the following: the amplitude of the deformation changes drastically the distribution of relaxation times as compared to the initial nondeformed system (Payne effect). The higher harmonic contributions are the results of fluctuations of the distribution of relaxation times during one period, and are a much smaller effect. The behavior of filled elastomers is at odds compared to systems which could be described by a nonlinear and nonretarded constitutive relation of the type $\sigma(x) = k^{(1)}x + k^{(3)}x^3 + k^{(5)}x^5 + ...$, for which there might be no possible distinction between the nonlinear behavior and the higher harmonics contributions. It appears thus that the glassy layer picture is able to explain various aspects of the mechanical behavior of filled elastomers: the reinforcement amplitudes; the Payne effect;[51] the recovery effects and specific features of the plastic properties of filled elastomers,[50,52] and the small—though not negligible—nonharmonic behavior of filled elastomers.

VIII. APPENDIX

The family of the Chebyshev polynomials of the first kind, T_n, form an Hilbertian basis of the $L^2[-1, +1]$ Hilbert space of

dx.doi.org/10.1021/ma202278e | Macromolecules 2012, 45, 2891−2904

squared integrable functions defined on [−1, +1], the corresponding scalar product being defined by:[73,74]

$$(f, g) = \int_{-1}^{+1} \frac{f(x)g(x)}{(1 - x^2)^{1/2}}\, dx \tag{24}$$

This means that (a) these polynomials satisfy to the orthogonal relations

$$(T_n, T_m) = \int_{-1}^{+1} \frac{T_n(x)T_m(x)}{(1 - x^2)^{1/2}}\, dx = \frac{\pi}{2}\delta_{n,m} \tag{25}$$

where $\delta_{n,m}$ is the Kronecker symbol which is one when $n = m$ and zero otherwise, (b) any function of $L^2[-1, +1]$ can be written in a unique way as an expansion

$$f(x) = \sum_{n=0}^{\infty} f_n T_n(x) \tag{26}$$

with

$$f_n = \frac{2}{\pi} \int_{-1}^{+1} \frac{T_n(x)f(x)}{(1 - x^2)^{1/2}}\, dx \tag{27}$$

The basic properties of these polynomials and their recursive relations, as well as the tabulation of the first of them are given in ref 74.

AUTHOR INFORMATION

Corresponding Author

*E-mail: samy.merabia@univ-lyon1.fr; didier.long-exterieur@eu.rhodia.com.

Notes

The authors declare no competing financial interest.

ACKNOWLEDGMENTS

The Ph.D. thesis of A.P. has been funded by Rhodia.

REFERENCES

(1) Nielsen, L. E.; Landel, R. F. *Mechanical Properties of Polymers and Composites*: Marcel Dekker: New York, 1994.
(2) Medalia, A. I. *Rubber Chem. Technol.* **1986**, *60*, 45−61.
(3) Edwards, D. C. *J. Mater. Sci.* **1990**, *25*, 4175−4185.
(4) Harwood, J. A. C.; Mullins, L.; Payne, A. R. *J. Appl. Polym. Sci.* **1965**, *9*, 3011−3021.
(5) Kraus, G. *Rubber Chem. Technol.* **1978**, *51*, 297−321.
(6) Kraus, G. *J. Appl. Polym. Sci. Appl. Polym. Symp.* **1984**, *39*, 75−92.
(7) Medalia, A. I. *Rubber Chem. Technol.* **1978**, *51*, 437−523.
(8) Payne, A. R. *J. Appl. Polym. Sci.* **1963**, *7*, 873.
(9) Payne, A. R. *J. Appl. Polym. Sci.* **1965**, *9*, 1073−1082.
(10) Heinrich, G.; Kluppel, M. *Adv. Polym. Sci.* **2002**, *160*, 1−44.
(11) Wang, M. J. *Rubber Chem. Technol.* **1998**, *71*, 520−589.
(12) Payne, A. R. *J. Appl. Polym. Sci.* **1962**, *21*, 368−372.
(13) Heinrich, G.; Kluppel, M.; Vilgis, T. A. *Reinf. Elastomers* **2002**, *6*, 195−203.
(14) Rendek, M.; Lion, A. *Zamm-Z. Angew. Math. Mech.* **2010**, *90*, 436−458.
(15) Rendek, M.; Lion, A. *KGK, Kautsch. Gummi Kunstst.* **2009**, *62*, 463−470.
(16) Lion, A.; Kardelky, C.; Haupt, P. *Rubber Chem. Technol.* **2003**, *76*, 533−547.
(17) Lion, A. *Continuum Mech. Thermodyn.* **1996**, *8*, 153−169.
(18) Hofer, P.; Lion, A. *J. Mech. Phys. Solids* **2009**, *57*, 500−520.
(19) Bueche, F. *J. Appl. Polym. Sci.* **1961**, *15*, 271−281.
(20) Berriot, J.; Lequeux, F.; Montès, H.; Monnerie, L.; Long, D.; Sotta, P. *J. Non-Cryst. Solids* **2002**, *307*, 719−724.
(21) Berriot, J.; Montes, H.; Lequeux, F.; Long, D.; Sotta, P. *Macromolecules* **2002**, *35*, 9756−9762.
(22) Berriot, J.; Montes, H.; Lequeux, F.; Long, D.; Sotta, P. *Europhys. Lett.* **2003**, *64*, 50−56.
(23) Montes, H.; Lequeux, F.; Berriot, J. *Macromolecules* **2003**, *36*, 8107−8118.
(24) Montes, H.; Chaussée, T.; Papon, A.; Lequeux, F.; Guy, L. *EPJE* **2010**, *31*, 263−268.
(25) Kaufmann, S.; Slichter, W. P.; Davis, D. D. *J. Polym. Sci., Part A2* **1971**, *9*, 829−839.
(26) Haidar, B.; Salah Deradji, H.; Vidal, A.; Papirer, E. *Macromol. Symp.* **1996**, *108*, 147−161.
(27) Tsagaropoulos, G.; Eisenberg, A. *Macromolecules* **1995**, *28*, 6067−6077.
(28) Tsagaropoulos, G.; Eisenberg, A. *Macromolecules* **1995**, *28*, 396−398.
(29) Tsagaropoulos, G.; Kim, J.-S.; Eisenberg, A. *Macromolecules* **1996**, *29*, 2222−2228.
(30) Struik, L. C. E. *Polymer* **1987**, *28*, 1521−1533.
(31) Wallace, W. E.; van Zanten, J. H.; Wu, W. L. *Phys. Rev. E.* **1995**, *52*, R3329.
(32) van Zanten, J. H.; Wallace, W. E.; Wu, W. L. *Phys. Rev. E.* **1996**, *53*, R2053.
(33) Grohens, Y.; Brogly, M.; Labbe, C.; David, M.-O.; Schultz, J. *Langmuir* **1998**, *14*, 2929−2932.
(34) Keddie, J. L.; Jones, R. A. L.; Cory, R. A. *Europhys. Lett.* **1994**, *27*, 59−64.
(35) Mattsson, J.; Forrest, J. A.; Borjesson, J. *Phys. Rev. E.* **2000**, *62*, 5187−5200.
(36) Hall, D. B.; Dhinojwala, A.; Torkelson, J. M. *Phys. Rev. Lett.* **1997**, *79*, 103−106.
(37) Long, D.; Lequeux, F. *EPJ E* **2001**, *4*, 371−387.
(38) Merabia, S.; Long, D. *EPJ E* **2002**, *9*, 195−207.
(39) Merabia, S.; Sotta, P.; Long, D. *EPJ E* **2004**, *15*, 189−210.
(40) Sotta, P.; Long, D. *EPJ E* **2003**, *11*, 375−388.
(41) Ellison, C. J.; Torkelson, J. M. *Nat. Mater.* **2003**, *2*, 695−700.
(42) Ciprari, D.; Jacob, K.; Tannenbaum, R. *Macromolecules* **2006**, *39*, 6565−6573.
(43) Putz, K.; Krishnamoorti, R.; Green, P. F. *Polymer* **2007**, *48*, 3540−3545.
(44) Kropka, J. M.; Putz, K. W.; Pryamitsyn, V.; Ganesan, V.; Green, P. F. *Macromolecules* **2007**, *40*, 5424−5432.
(45) Baeurle, S. A.; Usami, T.; Gusev, A. A. *Polymer* **2006**, *47*, 8604−8617.
(46) Rao, Y.-Q.; Pochan, J. M. *Macromolecules* **2007**, *40*, 290−296.
(47) Rittigstein, P.; Priestley, R. D.; Broadbelt, L. J.; Torkelson, J. M. *Nat. Mater.* **2007**, *6*, 278−282.
(48) Gusev, A. A. *Macromolecules* **2006**, *39*, 5960−5962.
(49) Kalfus, J.; Jancar, J. *Polymer* **2007**, *48*, 3935−3937.
(50) Merabia, S.; Sotta, P.; Long, D. R. *J. Polym. Sci., Part B: Polym. Phys.* **2010**, *48*, 1495−1508.
(51) Merabia, S.; Sotta, P.; Long, D. R. *Macromolecules* **2008**, *41*, 8252−8266.
(52) Chazeau, L.; Brown, J. D.; Yanyo, L. C.; Sternstein, S. S. *Polym. Compos.* **2000**, *21*, 202−222.
(53) Roland, C. M. *J. Rheol.* **1990**, *1*, 25−34.
(54) Leblanc, J. L. *Rubber Chem. Technol.* **2005**, *78*, 54−75.
(55) Leblanc, J. L. *J. Appl. Polym. Sci.* **2006**, *100*, 5102−5118.
(56) Wagner, M. H.; Rolon-Garrido, V. H.; Hyun, K.; Wilhelm, M. *J. Rheol.* **2011**, *55*, 495−516.
(57) Papon, A.; Montes, H.; Lequeux, F.; Guy, L. *J. Polym. Sci., Part B: Polym. Phys.* **2010**, *48*, 2490−2496.
(58) Cho, K. S.; Hyun, K.; Ahn, K. H.; Lee, S. J. *J. Rheol.* **2005**, *3*, 747−758.
(59) Leblanc, J. L. *Rubber Chem. Technol.* **2010**, *83*, 65−96.
(60) Klein, C. O.; Spiess, H. W.; Calin, A.; Balan, C.; Wilhem, M. *Macromolecules* **2007**, *40*, 4250−4259.
(61) Ewoldt, R. H.; Hosoi, A. E.; McKinley, G. H. *J. Rheol.* **2008**, *52*, 1427−1458.

(62) Ng, T. S. K.; McKinley, G. H. *J. Rheol.* **2011**, *55*, 627−654.
(63) Ewoldt, R. H.; Clasen, C.; Hosoi, A. E.; McKinley, G. H. *Soft Matter* **2007**, *3*, 634−643.
(64) Yu, W.; Wang, P.; Zhou, C. *J. Rheol.* **2009**, *53*, 215−238.
(65) Hyun, K.; Wilhelm, M.; Klein, C. O.; Cho, K. S.; Nam, J. G.; Ahn, K. H.; Lee, S. J.; Ewoldt, R. H.; McKinley, G. H. *Prog. Polym. Sci.* **2011**, *36*, 1697−1753.
(66) Wu, S. *Polym. Int.* **1992**, *29*, 229.
(67) Ferry, J. D. *Viscoelastic Properties of Polymers*: Wiley: New York, 1980.
(68) Merabia, S.; Long, D. *J. Chem. Phys.* **2006**, *125*, 234801.
(69) Long, D.; Sotta, P. *IMA Volume in Mathematics and its Applications: Modeling of Soft Matter*; Calderer, M.-C. T., Terentjev, E. M., Eds.; Springer Science+Business Media, Inc.: New York, 2005; Vol. *141*, pp 205−234.
(70) Long, D.; Sotta, P. *Macromolecules* **2006**, *39*, 6282−6297.
(71) Long, D.; Sotta, P. *Rheol. Acta* **2007**, *44*, 1029−1044.
(72) Mark, J. E. In *Physical Properties of Polymers Handbook*; American Institute of Physics: Melville, NY, 1996.
(73) Riesz, F.; Sz.-Nagy, B. *Functional Analysis*; Dover: New York, 1990.
(74) Abramowitz, M.; Stegun, I. A. *Handbook of Mathematical Functions*; Dover: New York, 1964.
(75) Gardel, M. L.; Shin, J. H.; MacKintosh, F. C.; Mahadevan, L.; Matsudaira, P.; Weitz, D. A. *Science* **2004**, *304*, 1301−1305.
(76) Ewoldt, R. H.; Hosoi, A. E.; McKinley, G. H. *Integr. Comp. Biol.* **2009**, *49*, 40−50.